Journal of Inorganic Biochemistry 270 (2025) 112938

Contents lists available at ScienceDirect

Journal of Inorganic Biochemistry

journal homepage: www.elsevier.com/locate/jinorgbio

Harnessing redox reactions for anticancer effects: A copper(II) Schiff base complex induces apoptosis in HepG2 liver cancer cells via ROS generation

Daniela Ganci [a], Luisa D'Anna [a], Giulia Abruscato [a], Malo Le Chevalier [b], Océane Quideau [c], Salvatore Cataldo [d], Alberto Pettignano [d], Simona Rubino [a], Roberto Chiarelli [a], Giampaolo Barone [a], Claudio Luparello [a,*], Riccardo Bonsignore [a,*]

[a] Dipartimento di Scienze e Tecnologie Biologiche, Chimiche e Farmaceutiche, Università degli Studi di Palermo, 90128 Palermo, Italy
[b] École Normale Supérieure Paris-Saclay, 91190 Gif-sur-Yvette, France
[c] Institut National des Sciences Appliquées de Rouen, 76800 Saint-Étienne-du-Rouvray, France
[d] Dipartimento di Fisica e Chimica – Emilio Segrè, Università degli Studi di Palermo, 90128 Palermo, Italy.

ARTICLE INFO

Keywords:
Copper(II) complex
Schiff base
Reactive oxygen species
Bioinorganic chemistry
Antitumour agents
HepG2

ABSTRACT

This study uncovers the potential of a copper(II) Schiff base complex, CuL^{2+}, to access the Cu(I) oxidation state and generate reactive oxygen species (ROS), highlighting its significance in eventual therapeutic applications. UV–vis absorption spectroscopy was used to follow the redox stability of the metal complex, also in the presence of reducing agents, such as ascorbic acid and glutathione, and of the copper(I) chelator, bathocuproine disulfonate. Utilizing human tumor cell lines HepG2 (hepatocarcinoma cells), we assessed its efficacy in reducing cell viability, increasing the sub-G_0/G_1 cell fraction, and initiating apoptotic pathways. Cell viability assays demonstrated a dose-dependent cytotoxicity with pronounced effects at sub-micromolar concentrations. Flow cytometry revealed significant ROS production, followed by mitochondrial membrane potential dissipation, and caspase activation, underscoring CuL^{2+}'s mechanism of action. These findings position CuL^{2+} as a promising candidate for cancer therapy, providing insights into copper complexes' therapeutic application through oxidative stress and apoptosis modulation.

1. Introduction

Copper, an essential trace element in the human body, is present in quantities of about 100 mg in an average individual [1,2]. In the +2 oxidation state, this metal ion plays a critical role in various enzymatic processes and cellular functions, including growth, cardiovascular integrity, lung elasticity, neovascularization, neuroendocrine function, and iron metabolism [3–6]. Similarly to other essential metal ions, due to copper's prominent role in the human body, humans have evolved mechanisms to overcome its overload [3–5]. Copper can therefore be less toxic to humans than non-essential exogenous metals, such as platinum containing drugs [7–11]. Leveraging on this and on its unique chemical and physical properties, researchers have developed various bioactive copper-containing compounds to treat a range of health conditions, including copper deficiency, inflammation, rheumatoid arthritis, and thrombotic diseases [12,13].

In general, copper homeostasis can be also targeted as a cancer vulnerability, with two main therapeutic approaches: i) using chelators to deplete copper pools that support tumor proliferation and metastasis; ii) using copper ionophores to increase copper ions and induce cuproptosis, a form of oxidative stress-induced cell death triggered by copper excess [14].

In recent decades, copper complexes have therefore emerged as promising candidates in the field of anticancer therapy [6,11,15] with the Casiopeinas family being the most clinically advanced, as they reached Phase I clinical trials in Mexico [16–18]. It should be noted that, together with several copper(II) complexes from phenanthroline-like ligands [19,20], many metal compounds from different ligands, including bipyridines [21,22], terpyridines [23–26], thiosemicarbazones [27–30], or Schiff bases [31–33], have shown promising anticancer properties in vitro.

Overall, copper(II) complexes employ multiple mechanisms to exert their anticancer effects, with a notable pathway involving the induction of oxidative stress via the generation of reactive oxygen species (ROS)

* Corresponding authors.
E-mail address: riccardo.bonsignore@unipa.it (R. Bonsignore).

https://doi.org/10.1016/j.jinorgbio.2025.112938
Received 2 December 2024; Received in revised form 28 April 2025; Accepted 29 April 2025
Available online 30 April 2025
0162-0134/© 2025 The Authors. Published by Elsevier Inc. This is an open access article under the CC BY license (http://creativecommons.org/licenses/by/4.0/).

[11,15]. ROS production, which leads to cancer cell death, is facilitated by the redox equilibrium of copper complexes between the copper(I) and copper(II) oxidation states, under physiological conditions. Additionally, control over speciation of the metal center is crucial for achieving the desired anticancer effect, as shown recently in the case of $CuPhenCl_2$ (Fig. 1) [34].

Besides ROS generation, potentially anticancer copper complexes inhibit topoisomerase I and II, disrupt proteasome function, and bind DNA, adding to their cytotoxic arsenal [11,15,35–38]. Moreover, they have also shown potent binding to G-quadruplexes (G4-DNA) [39–42], peculiar DNA conformations involved in cancer development and sustenance [43,44]. Intriguingly, the Schiff base metal complex CuL^{2+} (Fig. 1) has recently demonstrated tight and selective interactions with G4-DNAs, exhibiting binding constants nearly an order of magnitude higher than those of analogous compounds, such as ZnL^{2+} (Fig. 1) [39]. Despite this, the metal complex was unable to stabilize the human telomeric G4-DNA structure, likely due to the absence of favorable stacking interactions with the G4 tetrads. Nevertheless, CuL^{2+} has also shown interesting catalytic capabilities in the oxidation of benzyl alcohols, when encapsulated in Zeolite Y [45]. Building on this, we propose that CuL^{2+} may hold potential as an anticancer agent, given its catalytic activity which suggests the possibility to access to the +1 oxidation state, henceforth potentially inducing ROS production in cancer cells. By investigating its stability and redox behavior, in this manuscript we elucidate CuL^{2+} capability to generate ROS, which could be exploited to induce apoptosis in cancer cells. Through a series of in vitro assays, we examine the effects of CuL^{2+} on cell viability, cell cycle progression, and apoptotic pathways, using HepG2 liver cancer cells as a model system. Our findings aim to establish CuL^{2+} not only as a promising candidate for cancer therapy but also to provide insights into how copper redox equilibrium can be leveraged for therapeutic advantage.

2. Materials and methods

2.1. General

Solvents and reagents (reagent grade) were all commercially available and used without further purification. $CuL(ClO_4)_2$ was synthesized following a literature reported protocol [39] and its purity assessed via elemental analysis as it follows: $C_{14}H_{12}Cl_2N_6CuO_8$ ($CuL(ClO_4)_2$), exp. C 31.78 %, H 2.21 %, N 15.65 % (calc. C 31.92 %, H 2.30 %, N 15.96 %).

2.2. Spectroscopic studies

UV–vis spectra were collected using a Varian UV–vis Cary 1E double beam spectrophotometer equipped with a Peltier temperature controller. A 10 mM stock solution of the complex was prepared in DMSO and further diluted with water, ensuring that the organic solvent content in the final mixture never exceeded 0.005 %. UV–vis spectra of CuL^{2+} were recorded over 24 h, both alone and in the presence of 10 equivalents of ascorbic acid (AA) or glutathione (GSH), which were previously dissolved in water or in buffer Tris-HCl 1 mM (pH = 7.4) to achieve a final stock concentration of 10 mM. Additionally, UV–vis spectra of CuL^{2+} alone or in the presence of 10 equivalents of AA were recorded with the addition of 2 equivalents of bathocuproine disulfonate (BCS), either at the beginning of the measurements or after 24 h. Anaerobiotic experiments were repeated in the same conditions, using degassed water purged with N_2, and the reaction kept under a constant flow of N_2.

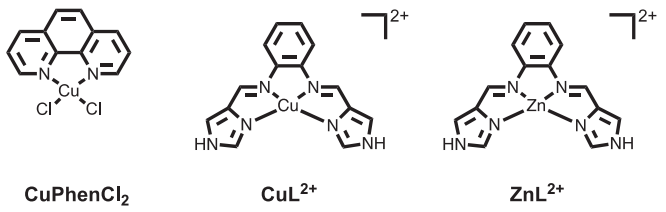

Fig. 1. Chemical structures of $CuPhenCl_2$ (Phen = 1,10-phenanthroline) and of the cationic copper(II) Schiff base complexes CuL^{2+} and ZnL^{2+} (L = N,N′-(1,2-phenylene)bis(1-(1*H*-imidazol-4-yl)methanimine)), both bearing two perchlorate anions as counterions.

The UV–vis spectrum of AA was recorded both independently and in the presence of 0.1 equivalents of CuL^{2+} and hydrogen peroxide (H_2O_2), maintained at a 10:1 ratio relative to AA. CuL^{2+} was prepared as a 5 mM stock solution in DMSO, while H_2O_2 was used as a 30 % solution, serving as a positive control. The experiments were conducted in 1 mM Tris-HCl buffer (pH = 7.4). The spectrum of AA alone was monitored over 24 h, whereas spectra recorded in the presence of CuL^{2+} and H_2O_2 were measured until the reaction reached completion, approximately one hour.

The Fluorescence-based detection of ROS was performed using 2′,7′-dichlorodihydrofluorescein (H_2DCF) as a probe in a 3.0 mL quartz fluorescence cuvette. A 12 mL working solution of H_2DCF 10 μM was prepared by deacetylation of H_2DCF-DA with 0.01 M NaOH and neutralization with 1 mM Tris-HCl buffer (pH 7.4). The reaction mixtures included a negative control with H_2DCF alone, a test sample with CuL^{2+} (stock solution in DMSO, final DMSO content ≤0.005 %), and a positive control with H_2O_2, both with a final concentration of 10 μM. Each mixture was brought to a final volume of 3.0 mL. Fluorescence measurements were performed using a spectrofluorometer FP-8300 with an excitation wavelength of 488 nm and an emission range of 495–600 nm and 525 nm band used to track ROS production. Fluorescence measurements were performed at two time points: immediately after sample preparation (t_0) and after 24 h storage in the darkness (t_{24}).

2.3. Electrochemical studies

Cyclic Voltammetry (CV) and Differential Pulse-Anodic Stripping Voltammetry (DP-ASV) experiments were carried out at room temperature (T = 298.15 K) by using a Metrohm 663 VA Stand (Series 05) workstation, equipped with a three electrode system supplied by Metrohm, consisting of: a Multimode Mercury Electrode (MME, code 6.1246.020) working in SMDE mode (Static Mercury Drop Electrode), a double junction Ag/AgCl/KCl (3 mol L-1) reference electrode (RE) (model 6.0728.120 + 6.1245.010), and a glassy carbon (GC) auxiliary electrode (AE) (model 6.1247.000 + 6.1241.020). The MME was filled with 99.9999 % Mercury (electronic grade, from Sigma-Aldrich). The workstation was connected to an Autolab potentiostat/galvanostat (Metrohm) with an IME663 interface (Metrohm). The whole system was controlled by NOVA v. 1.10 software (Metrohm). Purified N_2(g) was bubbled into the solutions for 300 s prior to any experiment.

CV and DP-ASV experiments were performed on 10 mL of solution containing the 1 mM CuL^{2+} solutions, $NaClO_4$ 0.1 M as supporting electrolyte and at pH = 7. Voltammograms were acquired with the freshly prepared CuL^{2+} solution and with the same solution after 24 h. Further CV and DP-ASV experiments were performed replacing the CuL^{2+} with $Cu(ClO_4)_2$ at the same concentration. CV experiments were carried out with the following scan conditions: starting potential = ending potential = − 0.300 V, upper vertex potential = 0.200 V, lower vertex potential = −0.600 V, number of stop crossings 3, step potential = 0.001 V, scan rate = 20 mV s^{-1}.

The working conditions of DP-ASV experiments were as follows: deposition potential = −0.600 V, deposition time = 1 s, equilibration time 10 s, start potential = −0.600 V, end potential = 0.200 V, step potential = 0.001 V, modulation amplitude = 0.05 V, interval time = 0.5 s, scan rate 20 mV s^{-1}.

2.4. Cell culture and viability test

HepG2 liver cancer cells were maintained in Dulbecco's modified Eagle medium (DMEM) supplemented with 10 % fetal bovine serum,

100 U/mL penicillin and 100 μg/mL streptomycin (Sigma, St.Louis, MO/USA), at 37 °C in a 5 % CO_2 atmosphere. For the viability assay, HepG2 cells in exponential growth were detached from the flasks with 0.05 % trypsin-EDTA, counted, seeded at the concentration of 5500 cells/well in 96-well plates, allowed to settle overnight, and grown in control conditions or in the presence of different concentrations of either CuL^{2+}, copper(II) acetate or the sole scaffold ranging from 10^{-3} to 10^{2} μM for 24 h. The trypan blue dye exclusion test was used to evaluate the number of viable cells [46,47]. The percent cell viability was determined as the ratio of the numbers of unstained cells between the treated and control conditions, and the half maximal inhibitory concentration (IC_{50}) was evaluated, using the CompuSyn software [48].

2.5. Flow cytometry

HepG2 cells were seeded in 6-well plates at a concentration of 88,000 cells/well and grown in control conditions or exposed to IC_{50} of CuL^{2+} for 24 h. Triplicate flow cytometric assays were performed as already reported [49,50] in a FACSCanto equipment (BD Biosciences, Franklin Lakes/NJ, USA), and 10,000 events were evaluated in each test. The obtained fcs files were analyzed with the Floreada tool available online at https://floreada.io (accessed on September 20th 2024). Gating in the FSC vs. SSC plot was performed to exclude cell debris, displaying low FSC values, from the results, whereas gating in the FSC-H vs. FSC-A plot was performed to exclude cell doublets and multiplets from the data of cell cycle analyses.

2.5.1. Cell cycle analysis

For the evaluation of the distribution of control and treated cells in the cycle phases, HepG2 cells were fixed with cold 70 % ethanol, exposed to 40 μg RNase A/mL, and stained with 20 μg propidium iodide (PI)/mL before analysis.

2.5.2. Apoptosis assay

The onset of apoptosis was checked through the binding of Annexin V-fluorescein isothiocyanate (FITC) to externalized phosphatidylserine. To this purpose, control and treated cells were labeled with Annexin V-FITC and PI as described by the manufacturer of the kit (Canvax Biotech, Cordoba, Spain). The percentages of live cells (Annexin V^- and PI^-), necrotic cells (Annexin V^- and PI^+) early-stage apoptotic cells (Annexin V^+ and PI^-) and late-stage/dead apoptotic cells (Annexin V^+ and PI^+) were determined.

2.5.3. Reactive oxygen species (ROS) assay

ROS generation in control and treated cells was determined with the ROS Detection Assay kit (Canvax Biotech), monitoring the extent of deacetylation and oxidation of the probe 2′,7′dichlorodihydrofluorescein diacetate into the fluorescent 2′,7′dichlorodihydrofluorescein, according to the manufacturer's instructions.

2.5.4. Mitochondrial membrane potential (MMP) measurement

To estimate their MMP status, control and treated cells were incubated with JC10 (Abcam, Cambridge, UK), a ratiometric fluorescent indicator sensitive to modifications of MMP, which aggregates in the mitochondrial matrix and undergoes a fluorescence emission shift from green (520 nm) to red (570 nm) in healthy cells, whereas it remains monomeric and stains cells green in the case of dissipation of MMP. A positive control containing 1 μM valinomycin, a K^+ ionophore which dissipates MMP, was included in the assay.

2.6. Caspase activity assay

HepG2 cells were seeded in 6-well plates at a concentration of 88,000 cells/plate and grown for 24 h in control conditions or exposed to IC_{50} of CuL^{2+}. Caspase activity was investigated using the Caspase Family Colorimetric Substrate kit II Plus (Abcam), following the manufacturer's instructions [46].

2.7. Detection of LDH release

For this assay the Lactate Dehydrogenase (LDH) Cytotoxicity Colorimetric Assay kit (Elabscience, Houston/TX, USA) was employed according to manufacturer's instructions. In brief, HepG2 cells were grown in control conditions or exposed to IC_{50} of CuL^{2+} for 24 h and then the supernatants of control and treated cells were drawn and incubated with the reaction working solution at 37 °C for 10 min. The optical density of each sample was determined at $\lambda = 450$ nm in a microplate reader.

2.8. Preparation of cell lysates and Western blot

Western blot analysis was performed as described elsewhere [46]. Essentially, trypsinized control and treated HepG2 cells were resuspended in a lysis buffer containing 7 M Urea, 2 % CHAPS, and 10 mM DTT, supplemented with a protease inhibitor cocktail (Sigma). Equal amounts of proteins were separated by 13 % sodium dodecyl sulphate-polyacrylamide gel electrophoresis (SDS-PAGE) and the protein bands transferred to nitrocellulose membranes. The blots were incubated with either primary antibody, i.e., rabbit gasdermin E (GSDME) antibody (A7432–20, ABclonal, Woburn/MA, USA; working dilution 1:750) or, as an endogenous control, rabbit actin antibody (Ab8227, Abcam; working dilution 1:1000) at 4 °C overnight. After exhaustive washing, the membranes were then incubated with the peroxidase-conjugated anti-rabbit secondary antibody (Ab6721, Abcam; working dilution 1:3000) at room temperature for 1 h. The protein bands were detected in a molecular imager (Versadoc MP Imaging System, Bio-Rad, Hercules, CA, USA) using the SuperSignal West Pico Plus substrate (ThermoFisher, Waltham, MA, USA) and quantitated used the Quantity One v.4.6.6 software (Bio-Rad).

2.9. Statistics

The normality tests were performed with SigmaPlot 11.0 software (SYSTAT, San Jose, CA, USA). For Western blot experiments, the data were analyzed by unpaired two-tailed Student's *t*-test using GraphPad Prism 9 software (GraphPad, San Diego, CA, USA).

3. Results and discussion

3.1. Stability, cu(I) accessibility, and redox potential of CuL^{2+}

As redox-activity is a key step for the antiproliferative effect of copper(II) complexes - according to our hypothesis - we assessed the stability of CuL^{2+} in water by monitoring the evolution of its UV–vis spectrum over time. To mirror the biological experimental conditions, CuL^{2+} was dissolved in DMSO, ensuring the percentage never exceeded 0.005 % in the experiments. The UV–vis spectrum of CuL^{2+} in water is characterized by two intense peaks at 305 and 315 nm, likely due to intraligand π-π* transitions, and a broad shoulder with three maxima at 347, 371, and 385 nm, attributable to infra-ligand transitions (black line in Fig. 2a-c).

Over 24 h, all these bands experienced a mild hypochromic effect, with the broad shoulder decreasing by approximately 14 % (Fig. 2a), indicating substantial stability of the compound under these experimental conditions. Interestingly, the absorbance decrease remained consistent regardless of whether the experiment was conducted in the presence or absence of O_2 (Fig. S1), demonstrating that the extent of the decrease is independent of oxygen availability. However, despite not being pronounced, the appearance of such an event can be attributed to several phenomena, ranging from solvent coordination to the $2+ \rightarrow 1+$ reduction of the metal center. To deepen the latter aspect, we examined the stability of CuL^{2+} in the presence of 10 equivalents of two reducing

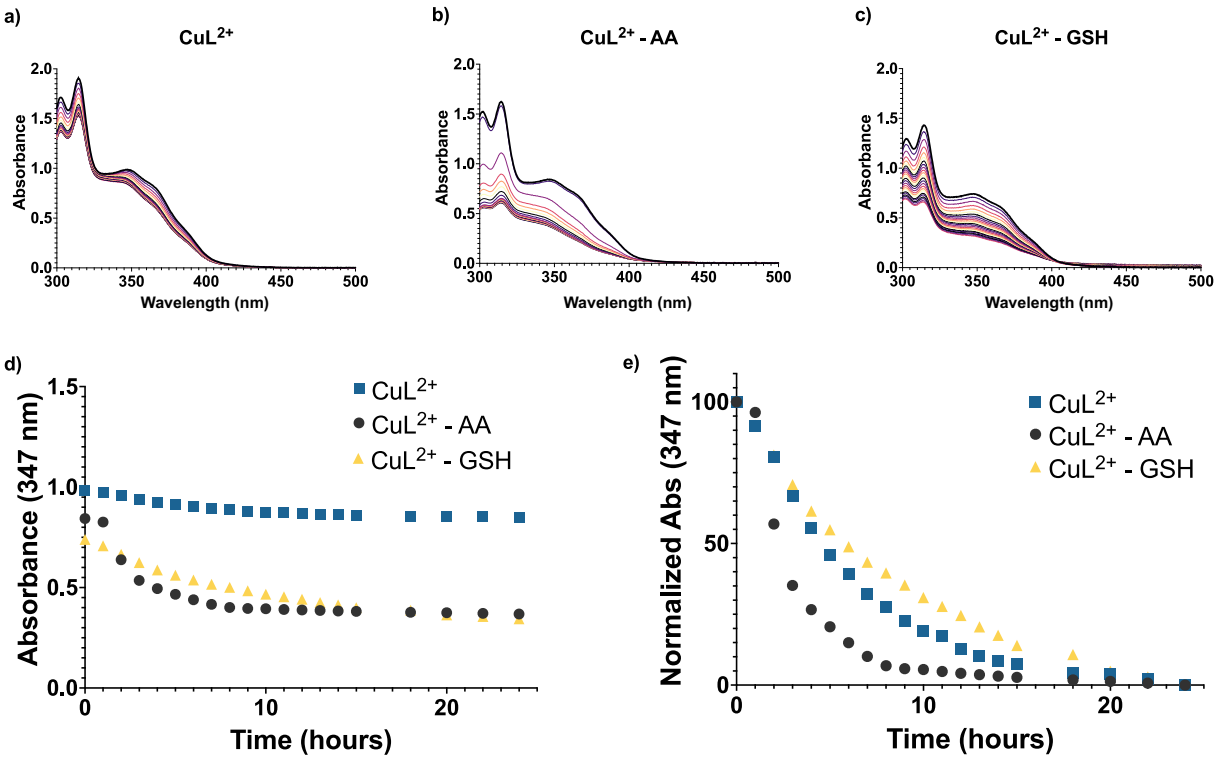

Fig. 2. UV–vis spectra of CuL^{2+} alone (a, $[CuL^{2+}] = 62.9$ μM, pH = 7.00) and in the presence of 10 equivalents of AA (b, $[CuL^{2+}] = 58.0$ μM, pH = 4.10) or GSH (c, $[CuL^{2+}] = 49.2$ μM, pH = 3.68) recorded in water over 24 h. The evolution of the 347 nm band and its normalization are shown in (d) and (e) respectively.

agents: AA and GSH, the latter chosen as model of physiologically relevant human reducing agents. Over 24 h, the UV–vis spectra of CuL^{2+} showed again a hypochromic effect, this time more pronounced than the one observed with the metal complex alone, with the band at 347 nm decreasing by nearly 57 % regardless of the reducing agent used (Fig. 2b and c). Intriguingly, the three solutions pH never changed during the experiments. Overall, this result suggests that in water, even in the absence of reducing agents, CuL^{2+} undergoes a spontaneous, very mild, one electron reduction of the metal center, as reported for other copper (II) complexes as those of phenantroline-like ligands [24]. Additionally, a comparison of the 347 nm band evolution in the three different experimental conditions is presented in Fig. 2d, while its normalized graph is plotted in Fig. 2e. These graphs confirm a comparable extent of hypochromism in the presence of both reducing agents but show that the decrease rate of the 347 nm band is much faster with AA, reaching a plateau after ca. 8 h. In contrast, with GSH the rate is similar to that of the compound alone, reaching a plateau only after ca. 19 h. Several factors contribute to the interpretation of this intriguing similarity, such as the redox mechanisms and the various species involved in the redox reactions.

Furthermore, the UV–vis spectra at 24 h for CuL^{2+} alone and in the presence of ascorbate or GSH revealed distinct features (Fig. S2). Despite the absorbance decrease, the shape of the CuL^{2+} UV–Vis spectrum (blue line in Fig. S2) remained relatively unchanged, while that in the presence of ascorbate exhibited a similar profile (red line in Fig. S2), suggesting an analogous overall behavior between these conditions. In contrast, the spectrum with GSH (green line in Fig. S2) showed a more pronounced change around 350 nm, indicating the formation of new species in solution: this behavior suggests that GSH likely displaces the Cu(I) ion, upon its formation, from the ligand, forming a Cu(I)-GSH complex [51], with the resulting UV–vis spectrum representing a combination of Cu(I)-GSH and unreacted CuL^{2+}. On the other hand, the similarity between the spectra of CuL^{2+} alone and CuL^{2+} with AA suggests that, in the latter case, the Cu(I) ion is formed without binding to AA.

To confirm the formation of Cu(I) species, following literature reported protocols [23,24,26], we repeated the stability kinetics in water in the presence of 2 equivalents of BCS, a well-known copper(I) chelator that forms a 2:1 (BCS:Cu^{+}) complex with a characteristic UV–vis band at 490 nm in water [23,24,26]. The addition of BCS to the CuL^{2+} solutions, either alone or with AA, resulted in the instantaneous appearance of the 490 nm band in the UV–vis spectra, reaching a plateau in both cases after 7 h (Fig. 3a-c). This confirms the formation of Cu(I) species, readily chelated by BCS. Intriguingly, however, the extent of $Cu(BCS)_2$ formation was comparable, with or without AA, which apparently contrasts with the weak decrease of the 347 nm band observed for the copper(II) complex when not exposed to any reducing agent.

To further investigate this aspect, the kinetics were repeated adding the BCS only after 24 h. The results, shown in Fig. 3d and e, clearly indicate that while the hypochromism is more pronounced with AA, as also observed in the previous experiments, the addition of BCS after 24 h equalizes the effect, resulting in similarly intense bands at 490 nm. Thus, it could be concluded that the use of BCS promotes the formation of Cu^{+} ions even in the absence of reducing agents: the presence of Cu^{+} stabilizing ligands, such as BCS, indeed, shifts towards right the $Cu^{2+} \leftrightharpoons Cu^{+}$ reduction equilibrium, to a similar extent than the presence of a strong reducing agent, such as AA.

We next evaluated the stability of the copper(II) complex in a near-physiological pH buffer, 1 mM Tris–HCl, pH 7.4. Under these conditions, the effects of AA and GSH on the complex's UV–Vis spectrum were largely consistent with those observed in water: both reductants caused a ~ 52 % decrease in the complex's 347 nm absorption band. Notably, even in the absence of any added reductant, the complex alone underwent a substantial loss (~50 %) of its 347 nm band intensity in the pH 7.4 buffer, essentially matching the decrease seen with AA or GSH (Fig. S3). After 24 h, addition of BCS led to the immediate appearance of a 490 nm band, confirming the formation of Cu(I) species from the complex (See inset in Fig. S3).

These observations indicate that the copper(II) center in CuL^{2+} can be spontaneously reduced to copper(I) even under mild, near-

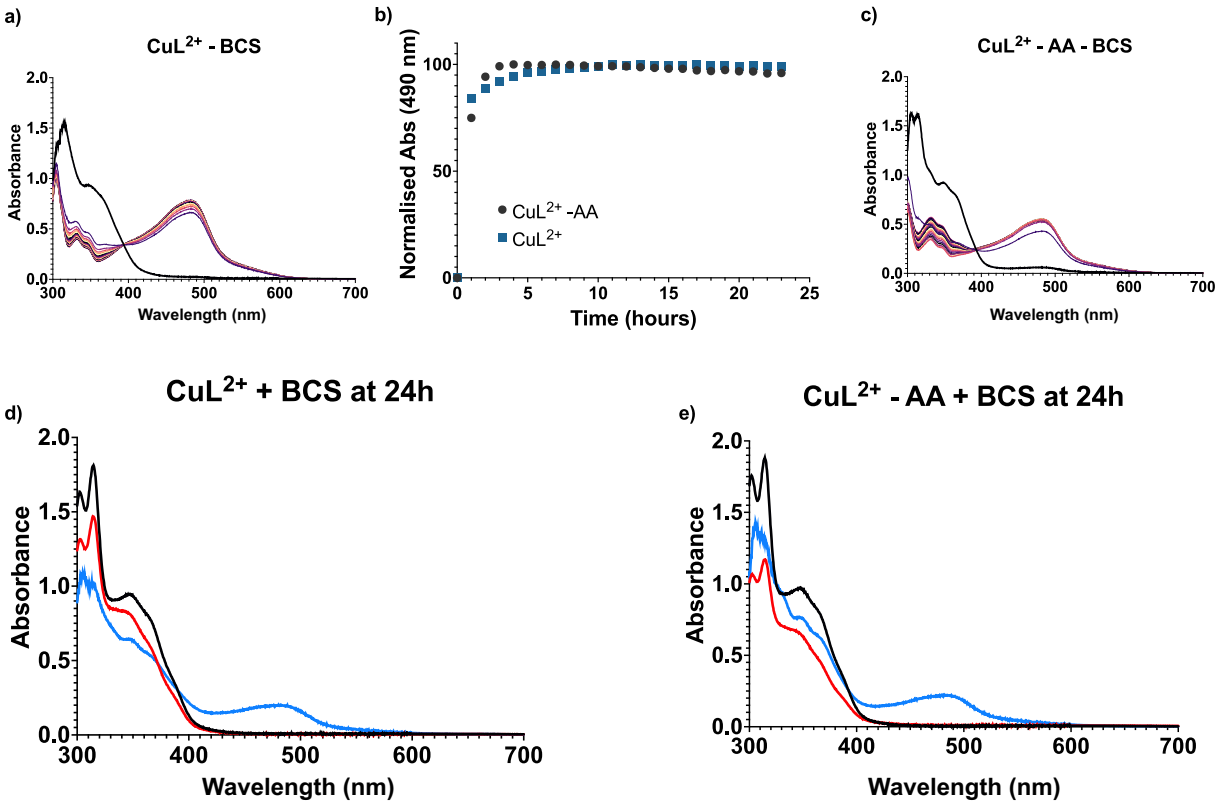

Fig. 3. UV–vis spectra of CuL^{2+} alone (a) and in presence of 10 equivalents of AA (c) in the presence of 2 equivalents of BCS, recorded in water over 24 h. (b) Normalized evolution of the 490 nm band. UV–vis spectra of CuL^{2+} alone (d) and in presence of 10 equivalents of AA (e) in recorded in water at 0 h (black curves), 24 h (red curves) and upon addition of 2 equivalents of BCS at 24 h (blue curves). (For interpretation of the references to colour in this figure legend, the reader is referred to the web version of this article.)

physiological conditions, suggesting that the complex could be inherently capable of oxidizing substrates of biological relevance under these in vitro conditions. To further probe this redox behavior, we monitored the oxidation of AA in the presence of CuL^{2+} by UV–Vis spectroscopy, using the same 1:10 CuL^{2+}:AA molar ratio as before (Fig. 4a,b and Fig. S4). We performed the experiment in 1 mM Tris–HCl (pH 7.4) to maintain physiological pH, and subtracting the complex UV–Vis spectrum to avoid spectral overlap with AA's absorbance. Under these conditions, AA alone exhibits a characteristic absorption maximum at 264 nm, which decreased by ~30 % over 24 h in the absence of the complex (Fig. S4). In the presence of CuL^{2+}, however, the 264 nm AA-band diminished completely within about 25 min. This rapid loss of AA absorbance is markedly faster than the effect of an equimolar amount of H_2O_2, which required roughly 40 min to produce a similar decrease at 264 nm (Fig. 4a,b). Thus, CuL^{2+} accelerates AA oxidation significantly, indicating efficient $Cu^{2+} \rightarrow Cu^{1+}$ reduction during the process and demonstrating a redox activity comparable to that of H_2O_2 under the same conditions.

Although the accelerated AA oxidation underscores the complex's strong redox activity, one could argue that the presence of a reducing agent (AA) might bias the system. We therefore employed a reactive oxygen species (ROS) detection assay (the H_2DCF /DCF fluorescence assay) to evaluate whether CuL^{2+} alone can generate ROS. In this assay, non-fluorescent H_2DCF is oxidized to fluorescent DCF, providing a validated readout of ROS generation. Samples containing H_2DCF were incubated with or without CuL^{2+} (1 or 5 equivalents) in 1 mM Tris–HCl (pH 7.4), and fluorescence (Ex = 488 nm, Em = 525 nm) was measured at $t = 0$ h and after 24 h. The experiment was further repeated using an equivalent amount of H_2O_2 as a positive control. Full emission spectra are provided in Fig. S5, and the increases in DCF fluorescence are summarized in Fig. 4c. As expected, in the absence of the complex, fluorescence remained negligible, confirming that H_2DCF does not oxidize to DCF on its own. By contrast, with 1 equivalent of CuL^{2+}, the DCF fluorescence increased by approximately 200-fold over 24 h. Using 5 equivalents of the complex did not produce a substantially higher signal, suggesting that the oxidative conversion reaches a plateau at around 1 equivalent of CuL^{2+}. Importantly, the magnitude of fluorescence increase observed with CuL^{2+} was comparable to that produced by H_2O_2, demonstrating that the complex can oxidize the H_2DCF substrate to a similar extent as a classical oxidant under these experimental conditions. Collectively, these experiments demonstrate that the copper (II) center in CuL^{2+} is readily reduced to copper(I) in aqueous solution at physiological pH, and that this enables ROS-mediated oxidation of substrates (including biologically relevant molecules like AA) under our experimental conditions.

To further investigate the redox behavior of CuL^{2+}, we complemented our spectroscopic analyses with electrochemical measurements using DP-ASV and CV techniques. These approaches are widely employed to probe metal–ligand interactions and redox stability by analyzing shifts in the deposition potential of electroactive metal centers [52,53]. In our study, DP-ASV measurements were performed on Cu $(ClO_4)_2$, a freshly prepared CuL^{2+} solution, and the same CuL^{2+} solution after 24 h, using 0.1 M $NaClO_4$ as supporting electrolyte. As shown in Fig. S6a, the freshly prepared CuL^{2+} solution displayed a negative shift in peak potential and a decrease in its height compared to free copper (II), indicating successful coordination with the ligand. After 24 h, the voltammogram revealed the disappearance of the initial peak in favor of two new signals, which are consistent with changes in the redox environment of the metal center, likely due to partial copper(II) reduction over time.

These findings were further supported by CV analysis (Fig. S6b), which showed shifts in both anodic and cathodic peaks for the CuL^{2+}

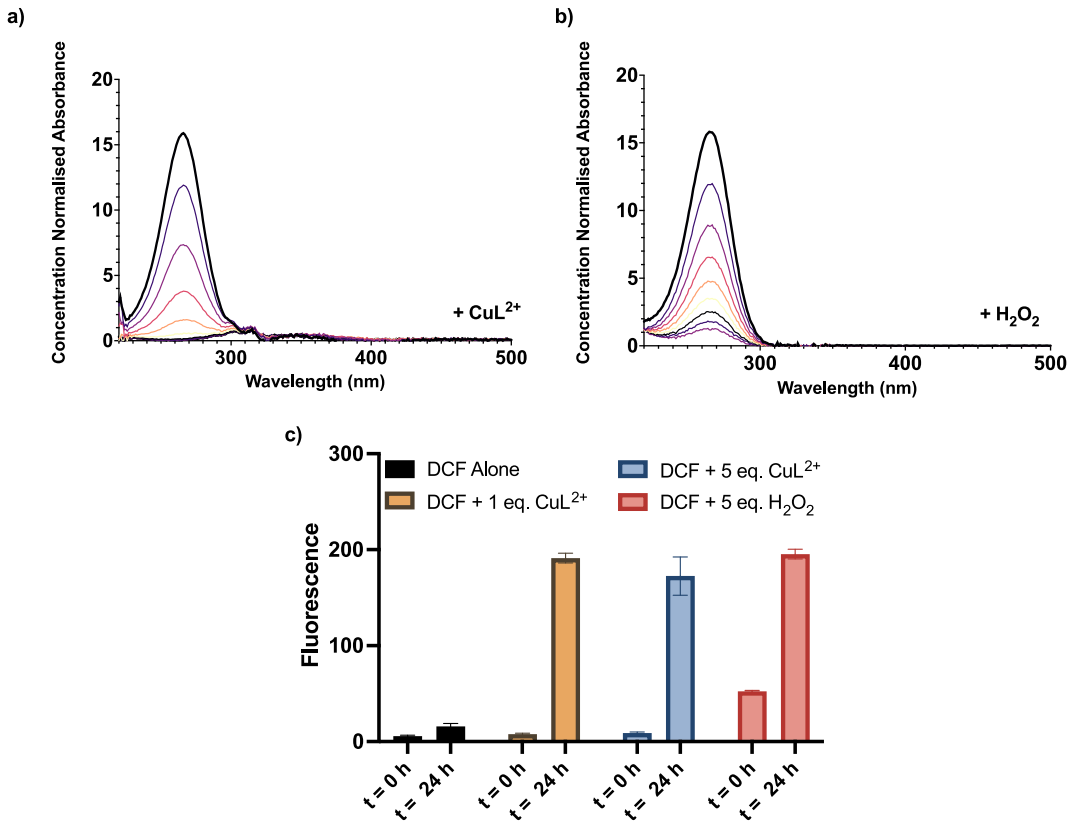

Fig. 4. UV–vis spectra of 10 eq. of AA in the presence of 1 eq. of CuL^{2+} (a) or H_2O_2 (b) recorded in buffer Tris-HCl 1 mM, pH = 7.4, every 5 min. (c) Fluorescence intensity of the 525 nm of DCF recorded in buffer Tris-HCl 1 mM, pH = 7.4, at $t = 0$ and 24 h in the presence of CuL^{2+} (1 or 5 eq.) or H_2O_2 (5 eq.); DCF fluorescence evolution when alone is reported in the black histogram.

complex compared to the free copper(II) salt, confirming coordination. The voltammogram recorded after 24 h indicated a modification in the complex redox profile, while still maintaining features consistent with a coordinated metal center. Additionally, the redox process appeared to be quasi-reversible under the experimental conditions, as reported for a similar copper(II) salen complex [54]. However, due to the use of a mercury drop working electrode, the accessible potential window was narrow, limiting the voltametric studies to the solely copper(II) - copper (I) couple. Overall, these electrochemical results are in excellent agreement with our UV–Vis and fluorescence-based data, further confirming the redox-active nature of CuL^{2+} and its ability to access the Cu (I) oxidation state over time.

In light of the reducing conditions present in some cancer and their capabilities to deplete Cu^{+} ions by forming ROS, we chose to investigate next the anticancer effects of the copper(II) complex.

3.2. CuL^{2+} induces the dose-dependent decrease of HepG2 cell viability

To gain information on these properties, we decided to test CuL^{2+} antiproliferative effects on HepG2 cells viability via trypan blue exclusion test and compare them with those of copper(II) acetate and the sole Schiff base ligand (L). It should be noted that, even though UV–Vis measurements were performed in 1 mM Tris–HCl buffer (pH 7.4), similar studies in DMEM could not be carried out due to medium instability under irradiation (see Fig. S7). Cell exposure for 24 h to CuL^{2+} at concentrations ranging from 0.001 to 100 μM resulted in a dose-dependent decrease in cell viability (Fig. 5). The mean IC_{50} was estimated as 0.078 μM and such concentration was utilized in all the subsequent biological experiments aimed to gather more detailed information on the molecular aspects of CuL^{2+}-induced toxicity on HepG2 cells. Notably, this value is respectively two and three orders of magnitude lower than the IC_{50} determined on the same cells for

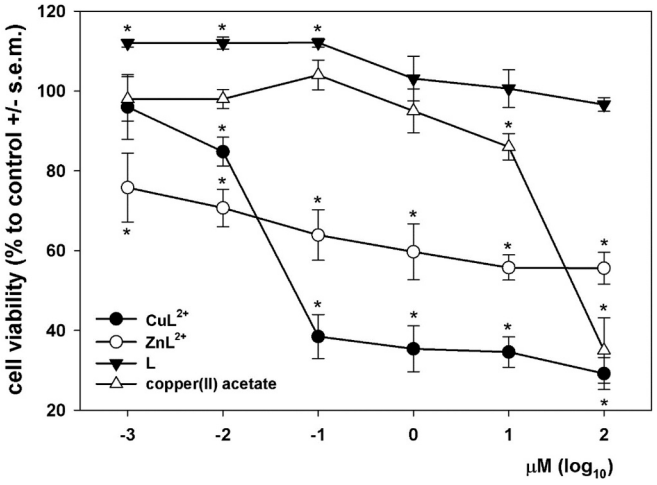

Fig. 5. Dose-response effect of CuL^{2+}, ZnL^{2+}, copper(II) acetate and the Schiff base ligand (L) on the viability of HepG2 cells. Cells were treated for 24 h with the compounds at the concentration range from 10^{-3} to 10^{2} μM and cell viability was assessed by trypan blue exclusion assay. The error bars correspond to the standard error of the mean (s.e.m.) of three independent measurements. *normality test vs. control passed. (For interpretation of the references to colour in this figure legend, the reader is referred to the web version of this article.)

phenantroline-based copper(II) complexes, including $CuPhenCl_2$ [55,56], and cisplatin [57]. This result highlights a potent anticancer effect of the copper(II) complex. Furthermore, no viability-restraining effect was exerted by the sole ligand at all the concentrations tested, whereas a prominent viability decrease was observed only with the

highest concentration of copper(II) acetate (i.e., 100 μM), which was not included in the following assays. These results collectively indicate that the anticancer properties of CuL^{2+} are not merely a simple combination of the effects of the ligand and metal ion alone. Instead, the entire complex, with its distinct physicochemical properties, plays a significant role in its anticancer activity. Unlike CuL^{2+}, a much flatter dose-response curve was obtained after cellular exposure to different doses of the redox inactive complex ZnL^{2+}, being cell viability reduced only by about 45 % at the highest concentration tested. Thus, the biological effect of ZnL^{2+} on the cell model under study appears more limited, likely based upon a different molecular impairment and/or restricted only to a subpopulation of the tumor cell line.

3.3. CuL^{2+} induces the accumulation of HepG2 cells in the sub-G_0G_1 fraction

In a further set of experiments, we checked whether perturbation was induced on HepG2 cell cycle by treatment with CuL^{2+}. To this purpose, the cells exposed to the IC_{50} of the compound for 24 h were stained with propidium iodide and submitted to flow cytometric analysis of the distribution of cells in the different cycle phases. Untreated cells showed a normal cell cycle with low sub-G_0/G_1 DNA peak. The presence of the CuL^{2+} determined the increase in sub-G_0/G_1 cell fraction and the global decrease in the population of cells in G_0/G_1, S and G_2/M phases (Fig. 6a). Analysis of the distribution of cell fractions in the cycle phases in triplicate assays underscored that CuL^{2+} did not affect the cycle progress as shown by the absence of significant variations of the percent distribution of live cells in G_0/G_1, S and G_2/M phases (Fig. 6b). On the other hand, after exposure to CuL^{2+} a six-fold ca. increase of the sub-G_0/G_1 cells amount, which includes dying cells that have undergone DNA fragmentation and the quota of cellular debris, could be observed (Fig. 6c).

3.4. CuL^{2+} leads HepG2 cells to apoptotic death involving the activation of caspase-3 and -5

To get more insight into the mechanism of CuL^{2+} cytotoxicity, the apoptosis-related surface exposure of phosphatidylserine in treated and control cell samples was investigated through its affinity to FITC-labeled annexin V. The cell suspension was counterstained with PI before the flow cytometric assay as a marker of the intactness of cell membranes. As shown in Fig. 7, in line with the previous data regarding the increase of the sub-G_0/G_1 cell population, after 24 h of exposure to CuL^{2+} IC_{50} the percentage of the viable annexin V^-/PI^- cells decreased from about 88 % of the controls to about 59 % and, on the other hand, the percentage of the apoptotic annexin V^+/PI^+ cells increased from about 6 % of the controls to about 35 %, to a similar extent than the above-mentioned copper(II) phenantholine-based complex [55]. No significant differences were found between both the early apoptotic annexin V^+/PI^- and the necrotic annexin V^-/PI^+ cell populations whose percentage remained low (below 4 %) under any experimental condition, overall suggesting the apoptotic death occurrence of the treated cells.

Furthermore, to get more information on the activity of the caspase proteases involved in CuL^{2+}-triggered cytotoxicity, treated and control cell lysates were submitted to the spectrophotometric quantitation (λ = 405 nm) of the free para-nitroaniline (pNA) release by cleavage of the pNA-labeled substrates for caspase-1, −2, −3, −5, −6, −8 and − 9. As shown in Fig. 8, CuL^{2+} treatment induced the activation of the apoptotic caspase-3 and the inflammatory caspase-5, whereas no statistically relevant result was obtained for the other enzymes.

Caspase-3 is an executioner caspase and its activation by both the extrinsic and intrinsic apoptotic pathways determines the occurrence of apoptosis-associated cellular events, including the observed translocation of phosphatidylserine to the external leaflet of the membrane. An interaction between caspase-3 and -5 leading to their mutual

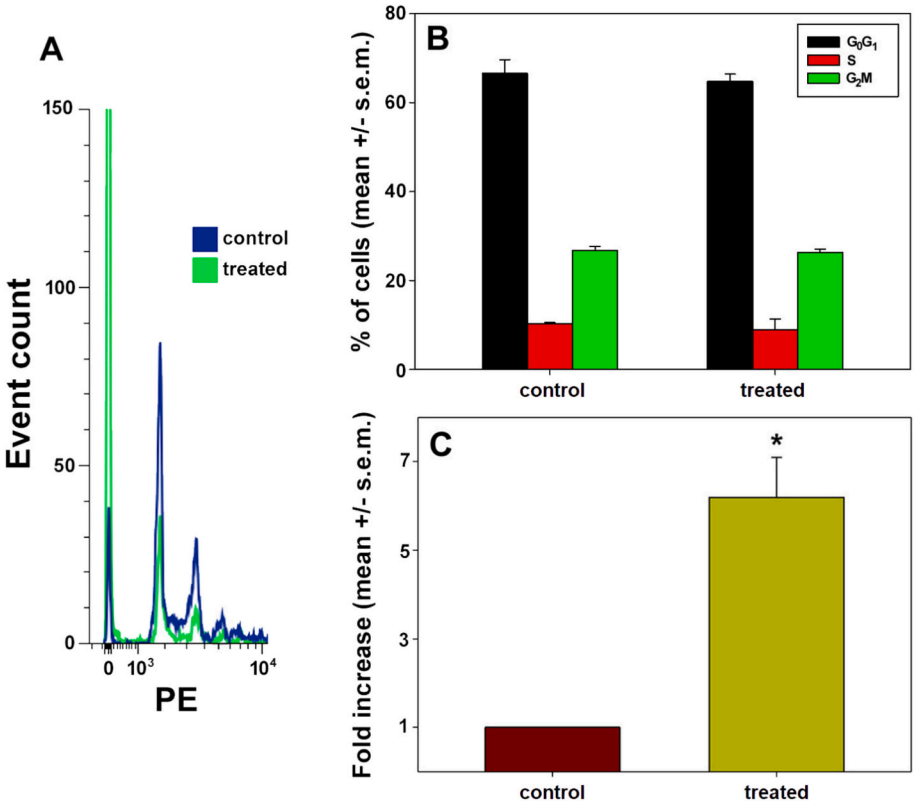

Fig. 6. A) Cell cycle profiles of control and CuL^{2+}-treated HepG2 cells. B) and C) Bar graphs showing the distribution of control and CuL^{2+}-treated HepG2 cells in the cell cycle phases (B) and the increase of the percentage of treated cells in the sub-G_0/G_1 fraction compared to control (C). The error bars indicate the standard error of the mean (s.e.m.) of three independent measurements. *normality test vs. control passed.

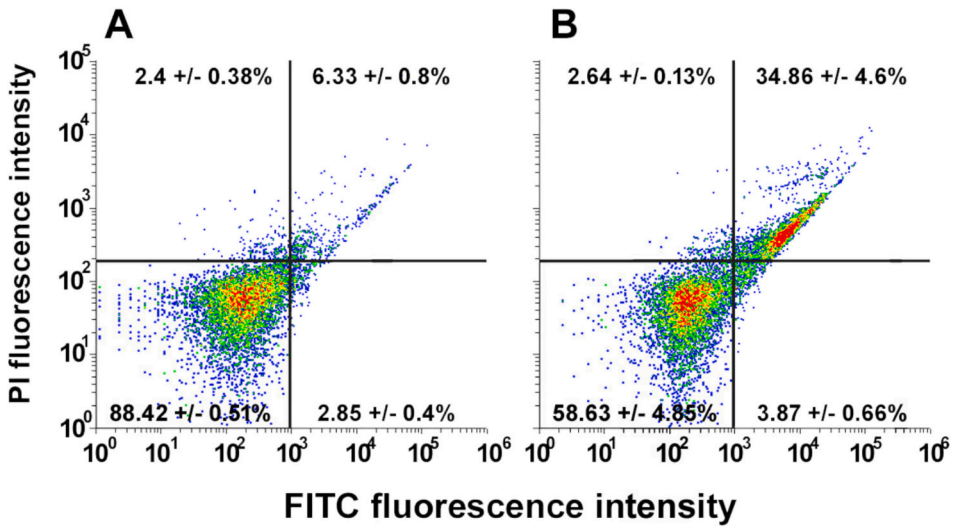

Fig. 7. Flow cytometric assays for apoptosis in HepG2 cells cultured in control conditions or exposed to CuL^{2+} IC_{50} for 24 h. The plots show the results of representative experiments and the percentages, indicated as the mean ± s.e.m. of three independent experiments, refer to viable annexin-V^-/PI^- cells (bottom left quadrant), early apoptotic annexin-V^+/PI^- cells (bottom right quadrant), late apoptotic annexin-V^+/PI^+ cells (top right quadrant) and necrotic annexin-V^-/PI^+ cells (top left quadrant).

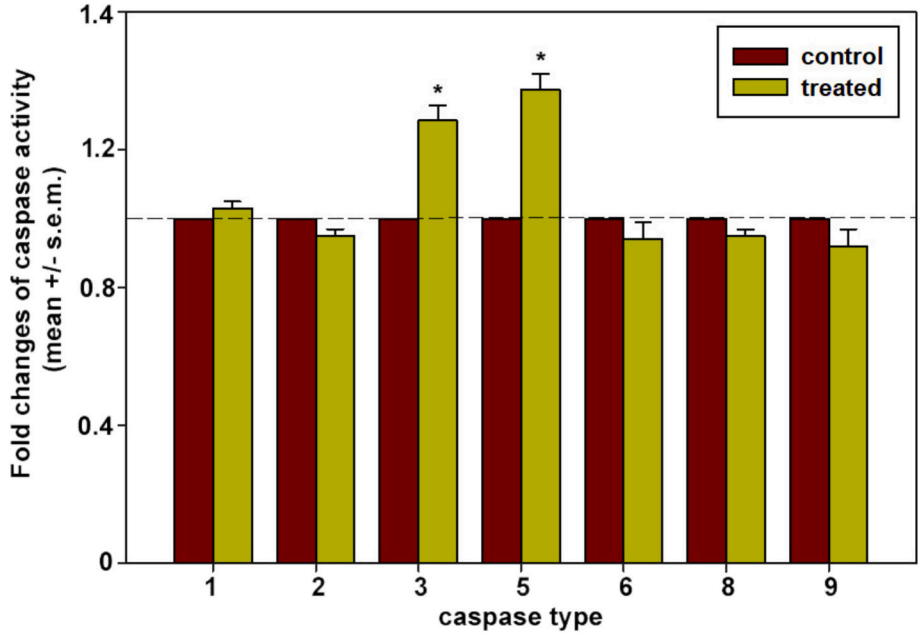

Fig. 8. Caspase activity determination in HepG2 cells cultured in control conditions or exposed to the IC_{50} of CuL^{2+} for 24 h. The error bars indicate the standard error of the mean (s.e.m.) of three independent measurements. * normality test vs. control passed.

activation in apoptosis has been reported; in addition, both caspases has been found involved in the switching-on of the pyroptotic pathway [49,50]. Pyroptosis is a form of programmed cell death promoted by proteins of the gasdermin (GSDM) family whose pore-forming N-terminal domains, when activated by cleavage, induce plasma membrane permeabilization followed by cell swelling and release of inflammatory factors [58]. To check the possible contribution of pyroptosis in the cytotoxic effect of CuL^{2+} on HepG2 cells we measured by Western blot the expression and cleavage of GSDME, the effector protein of caspase-3 in pyroptosis, liberating the GSDME-N domain. Additionally, we also evaluated the possible increase of LDH release due to the GSDME-N-mediated breakdown of the plasma membrane. The obtained results (Fig. 9) showed that, following treatment, a moderate increase of GSDME-N could be observed whereas no increase of LDH release was found (treated/control ratio = 99.05 +/− 2.25). This suggests that the modest amount of generated GSDME-N was not sufficient to trigger the pyroptotic damage leading to cell swelling, and that the activity of caspase-3 and -5 under the experimental conditions used was conceivably addressed to the realization of the sole apoptotic program.

3.5. CuL^{2+} induces the dissipation of the mitochondrial membrane potential ($\Delta\Psi m$) and the up-regulation of reactive oxygen species (ROS)

Considering the described ability of GSDME-N to permeabilize the mitochondrial membrane, thereby potentiating the activation of the intrinsic pathway of apoptosis [59], we investigated whether cell exposure to the compound could impair the mitochondrial function. Extensive damage to the mitochondria may indeed address cells to

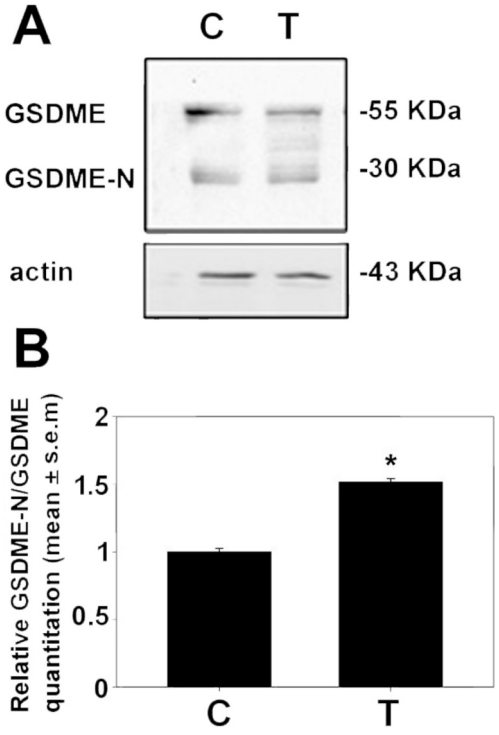

Fig. 9. A) Western blot analysis for GSDME and GSDME-N in control (C) and CuL^{2+}-treated (T) HepG2 cells (refer to Fig. S8 for the full view). B) Bar graph depicting the relative quantification obtained by band densitometry, normalized to actin, of three independent experiments of which the panel in (A) is representative. The error bars indicate the standard error of the mean (s.e.m.). * normality test vs. control passed.

apoptotic death [60]. The mitochondrial membrane potential ΔΨm status was therefore monitored with the cationic lipophilic JC10 dye which reversibly changes its fluorescent colour depending on mitochondrial polarization state, thereby evaluating the percentage of cells with intense red emission (indicative of intact ΔΨm) and of those ones with bright green/dim red emission (indicative of ΔΨm collapse). As shown in Fig. 10, cell treatment with IC_{50} CuL^{2+} for 24 h resulted in ΔΨm dissipation. In particular, the intense red-emitting cells were found to decrease from about 60 % of the negative controls (Fig. 10a) to about 3 % of the treated samples (Fig. 10b), closely matching the value obtained with the positive control treated for 24 h with valinomycin (about 0.16 %, Fig. 10c), a gold standard for ΔΨm evaluation [61].

Noteworthy, most intracellular ROS, which are known to play multiple roles in the maintenance of redox balance and in the regulation of intracellular signalization, are produced in the mitochondrial respiratory chain, although protein components located in other subcellular compartments, such as the endoplasmic reticulum, are involved in ROS generation [62]. Interestingly, due to their poor level of expression of *CYP2E1*, coding for cytochrome P450 family 2 subfamily E member 1, a ROS-generating enzyme of the endoplasmic reticulum, HepG2 cells represent a useful model to examine almost exclusively ROS generation from mitochondrial sources [63]. As CuL^{2+} has shown in vitro the potential accessibility to the +1 metal oxidation state, we deduce that the metal compound could have affected the mitochondrial respiratory chain by increasing the ROS levels. Hence, the production of diverse types of ROS (hydrogen peroxide, peroxynitrite, hydroxyl radicals, nitric oxide, and peroxy radicals) after 24 h of exposure to the metal complex IC_{50} was examined by flow cytometric analysis of the oxidation extent of the cell-permeant non-fluorescent 2′,7′-dichlorodihydrofluorescein diacetate (H_2DCFDA) to the poorly-permeant green fluorescence-emitting 2′,7′-dichlorofluorescein (DCF). The representative flow cytometric profile and the bar graphs shown in Fig. 11, demonstrate an about

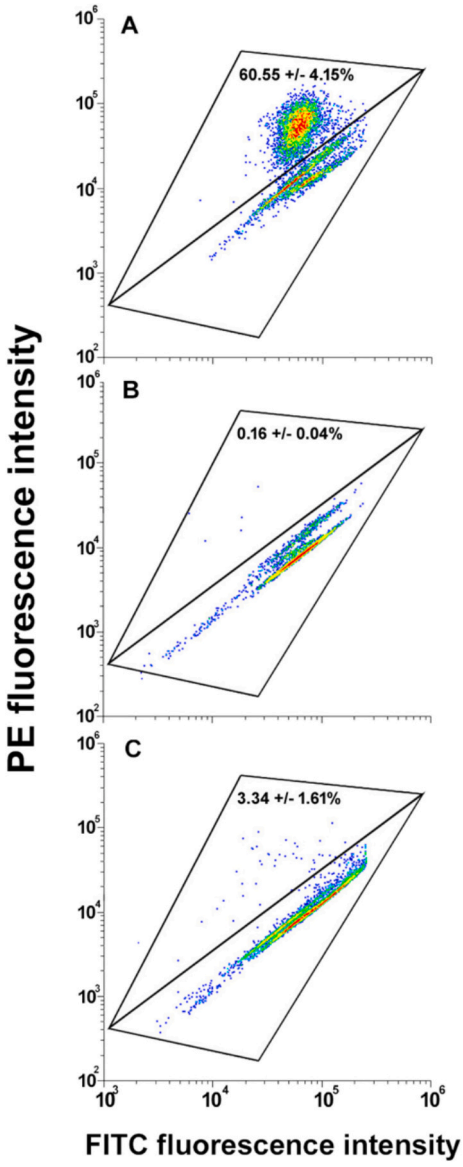

Fig. 10. Flow cytometric assays for MMP in HepG2 cells cultured for 24 h in control conditions (A), in the presence of 1 μM valinomycin (B), and of CuL^{2+} IC_{50}. The plots show the results of representative experiments and the percentages in each frame, indicated as the mean ± s.e.m. of three independent experiments, are referred to bright red-emitting cells that retain an intact MMP. (For interpretation of the references to colour in this figure legend, the reader is referred to the web version of this article.)

three-fold up-regulation of ROS in the presence of CuL^{2+} (average control cells' MFI vs. treated cells' MFI = 4309 vs. 13,080), strongly suggesting their involvement in HepG2 cells death.

4. Conclusions

In conclusion, this study demonstrates the dynamic redox behavior of the copper(II) complex CuL^{2+} and highlights its potential implications for anticancer activity. UV–Vis spectroscopy revealed that the complex undergoes a spontaneous reduction to Cu(I) over time, indicating an intrinsic redox activity capable of supporting ROS generation even in the absence of external reductants. While this process is notably accelerated in the presence of biological reducing agents such as ascorbic acid or glutathione in aqueous solution, experiments conducted under near-physiological conditions (1 mM Tris–HCl, pH 7.4) revealed a

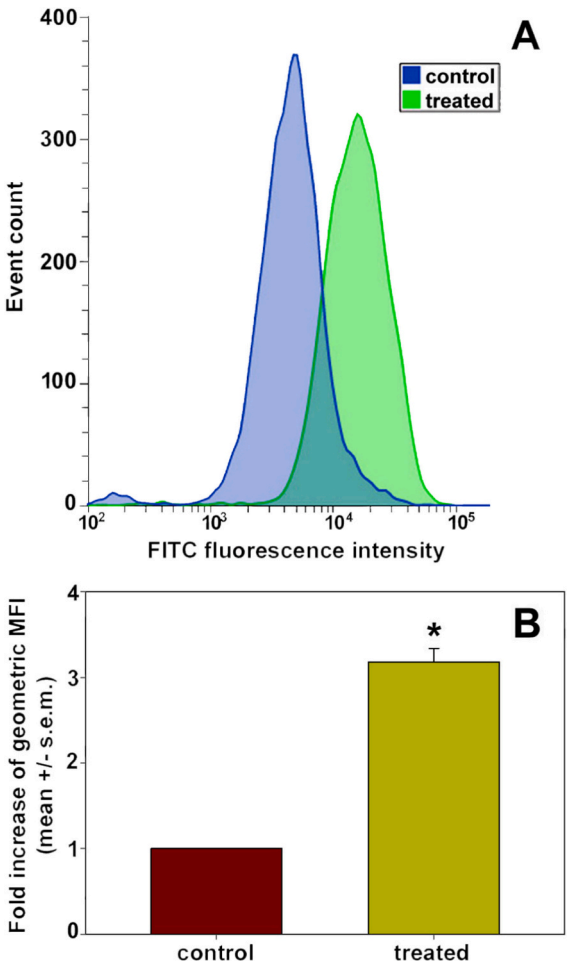

Fig. 11. A) Representative plots showing the accumulation of ROS in gated alive HepG2 cells treated with CuL^{2+} compared to control. The quantitative evaluation of the ROS-associated geometric mean fluorescence intensity (MFI) of control and treated cells is shown in the bar graph in B). The error bars indicate the standard error of the mean (s.e.m.) of three independent measurements. *normality test vs. control passed.

comparable extent of spectral change, regardless of whether a reducing agent was present. The BCS experiments further confirmed Cu(I) species formation, showing that even when the CuL^{2+} spontaneous reduction is limited, BCS effectively dissipates Cu(I) presence, shifting the reduction equilibrium to favor its production. These findings suggest that the redox activity of CuL^{2+} is not only robust but also enhanced in environments mimicking biological conditions, supporting its potential role in ROS-mediated cytotoxic mechanisms.

These in vitro results align with the mechanistic insights derived from cell-based studies, where CuL^{2+} was observed to induce substantial cellular stress in HepG2 cells. This is evidenced by significant ROS production, which disrupts cellular homeostasis. ROS generation leads to the dissipation of the mitochondrial membrane potential and initiates the apoptotic cascade through the activation of key caspases such as caspase-3 and -5. The increased accumulation of cells in the sub-G_0/G_1 phase, alongside the activation of apoptotic pathways, underscores the potent cytotoxic effects driven by CuL^{2+} redox transformation. These cellular disruptions highlight a promising strategy for targeting rapidly dividing cancer cells, offering a potential approach to overcoming oncogenic resilience by exploiting oxidative stress mechanisms.

Furthermore, optimizing CuL^{2+} offers a promising path for enhancing its selectivity and therapeutic potency. Structural modifications to the ligand framework represent a compelling strategy to fine-tune the redox properties of the complex. For instance, substituting differently decorated phenylene diamines or introducing electron-donating or electron-withdrawing groups o48n the ligand can influence the redox activity of the complex, improving its efficiency in generating ROS under biologically relevant conditions. Additionally, such modifications can enhance the complex's affinity for G-quadruplex DNA by altering its geometric and electronic properties. The use of planar aromatic ligands with extended π-conjugation, for example, could strengthen π-π stacking interactions with G4 structures, enabling dual-action efficacy through both redox-driven cytotoxicity and targeted DNA interactions. In parallel, synergistic combinations with existing chemotherapeutics could amplify the anticancer effects of CuL^{2+}, integrating the metal complex into multifaceted treatment regimens.

By linking the redox properties of CuL^{2+} to its biological effects and outlining strategies for its future development, this study provides new insights into the design of redox-active metal complexes as anticancer agents. These findings lay a strong foundation for further research aimed at improving the selectivity and efficacy of CuL^{2+}.

CRediT authorship contribution statement

Daniela Ganci: Writing – review & editing, Validation, Methodology, Investigation, Formal analysis. **Luisa D'Anna:** Methodology, Investigation, Formal analysis. **Giulia Abruscato:** Writing – review & editing, Investigation, Formal analysis. **Malo Le Chevalier:** Writing – review & editing, Investigation. **Océane Quideau:** Investigation. **Salvatore Cataldo:** Investigation, Formal analysis. **Alberto Pettignano:** Formal analysis. **Simona Rubino:** Writing – review & editing, Formal analysis. **Roberto Chiarelli:** Writing – review & editing, Investigation. **Giampaolo Barone:** Writing – review & editing, Funding acquisition. **Claudio Luparello:** Writing – review & editing, Writing – original draft, Supervision, Conceptualization. **Riccardo Bonsignore:** Writing – review & editing, Writing – original draft, Supervision, Funding acquisition, Conceptualization.

Declaration of competing interest

The authors declare that they have no known competing financial interests or personal relationships that could have appeared to influence the work reported in this paper.

Acknowledgements

The authors acknowledge funding from the European Union – NextGenerationEU through the Italian Ministry of University and Research D.M. 737/2021 – project "CuG4Ox". RB and LD acknowledge financial support of the National Recovery and Resilience Plan (PNRR) Mission 4 Component 2 Investment 1.1 – European Union-NextGenerationEU (grant PRIN PNRR 2022-P2022EMY52; CUP B53D23025640001; project title: "EnzyMime – Biocompatible and sustainable enzyme mimics based on metal complexes with peptide derivatives: synthesis, characterization and potential biological applications"). All the authors thank for financial support the European Union - NextGenerationEU through the Italian Ministry of University and Research under PNRR – Mission 4 Component 2 Investment 1.3 Project PE_00000019 "HEAL ITALIA" CUP (B73C22001250006).

Data availability

Data will be made available on request.

References

[1] A.C. Ross, B. Caballero, R.J. Cousins, K.L. Tucker, T.R. Ziegler, Modern Nutrition in Health and Disease: Eleventh Edition, 2012, pp. 1–1616, https://doi.org/10.1097/01.ccm.0000236502.51400.9f.

[2] J.L. Burkhead, J.F. Collins, Nutrition information brief-copper, Adv. Nutr. 13 (2022) 681–683, https://doi.org/10.1093/ADVANCES/NMAB157.

[3] N.R.C, (US) C. on C. in D. Water, Physiological Role of Copper. https://www.ncbi.nlm.nih.gov/books/NBK225407/, 2000 accessed November 5, 2024.

[4] Y. Li, J. Liang, Y. Chen, Y. Wang, The mechanism of copper homeostasis and its role in disease, ILABMED 1 (2023) 109–120, https://doi.org/10.1002/ILA2.22.

[5] S. Christgen, R.E. Tweedell, T.D. Kanneganti, Programming inflammatory cell death for therapy, Pharmacol. Ther. 232 (2022), https://doi.org/10.1016/J.PHARMTHERA.2021.108010.

[6] S. Abdolmaleki, A. Aliabadi, S. Khaksar, Unveiling the promising anticancer effect of copper-based compounds: a comprehensive review, J. Cancer Res. Clin. Oncol. 150 (2024) 213, https://doi.org/10.1007/s00432-024-05641-5.

[7] M. Carcelli, M. Tegoni, J. Bartoli, C. Marzano, G. Pelosi, M. Salvalaio, D. Rogolino, V. Gandin, In vitro and in vivo anticancer activity of tridentate thiosemicarbazone copper complexes: unravelling an unexplored pharmacological target, Eur. J. Med. Chem. 194 (2020) 112266, https://doi.org/10.1016/J.EJMECH.2020.112266.

[8] S.S. Massoud, F.R. Louka, N.M.H. Salem, R.C. Fischer, A. Torvisco, F.A. Mautner, J. Vančo, J. Belza, Z. Dvořák, Z. Trávníček, Dinuclear doubly bridged phenoxido copper(II) complexes as efficient anticancer agents, Eur. J. Med. Chem. 246 (2023) 114992, https://doi.org/10.1016/J.EJMECH.2022.114992.

[9] X. Man, W. Li, M. Zhu, S. Li, G. Xu, Z. Zhang, H. Liang, F. Yang, Anticancer tetranuclear cu(I) complex catalyzes a click reaction to synthesize a chemotherapeutic agent in situ to achieve targeted dual-agent combination therapy for cancer, Angew. Chem. Int. Ed. (2024) e202411846, https://doi.org/10.1002/ANIE.202411846.

[10] B. Kaya, H. Smith, Y. Chen, M.G. Azad, T.M. Russell, V. Richardson, P.V. Bernhardt, M. Dharmasivam, D.R. Richardson, Targeting lysosomes by design: novel N-acridine thiosemicarbazones that enable direct detection of intracellular drug localization and overcome P-glycoprotein (Pgp)-mediated resistance, Chem. Sci. 15 (2024) 15109–15124, https://doi.org/10.1039/D4SC04339A.

[11] C. Santini, M. Pellei, V. Gandin, M. Porchia, F. Tisato, C. Marzano, Advances in copper complexes as anticancer agents, Chem. Rev. 114 (2014) 815–862, https://doi.org/10.1021/CR400135X.

[12] O. Krasnovskaya, A. Naumov, D. Guk, P. Gorelkin, A. Erofeev, E. Beloglazkina, A. Majouga, Copper coordination compounds as biologically active agents, Int. J. Mol. Sci. 21 (2020), https://doi.org/10.3390/IJMS21113965.

[13] I. Iakovidis, I. Delimaris, S.M. Piperakis, Copper and its complexes in medicine: a biochemical approach, Mol. Biol. Int. 2011 (2011) 1–13, https://doi.org/10.4061/2011/594529.

[14] E.J. Ge, A.I. Bush, A. Casini, P.A. Cobine, J.R. Cross, G.M. DeNicola, Q.P. Dou, K. J. Franz, V.M. Gohil, S. Gupta, S.G. Kaler, S. Lutsenko, V. Mittal, M.J. Petris, R. Polishchuk, M. Ralle, M.L. Schilsky, N.K. Tonks, L.T. Vahdat, L. Van Aelst, D. Xi, P. Yuan, D.C. Brady, C.J. Chang, Connecting copper and cancer: from transition metal signalling to metalloplasia, Nat. Rev. Cancer 22 (2) (2021) 102–113, https://doi.org/10.1038/s41568-021-00417-2.

[15] C. Marzano, M. Pellei, F. Tisato, C. Santini, Copper complexes as anticancer agents, Anti Cancer Agents Med. Chem. 9 (2009) 185–211, https://doi.org/10.2174/187152009787313837.

[16] I. Gracia-Mora, L. Ruiz-Ramírez, C. Gómez-Ruiz, M. Tinoco-Méndez, A. Márquez-Quiñones, L.R. De Lira, Á. Marín-Hernández, L. Macías-Rosales, M.E. Bravo-Gómez, Knigth's move in the periodic table, from copper to platinum, novel antitumor mixed chelate copper compounds, Casiopeinas, evaluated by an in vitro human and murine Cancer cell line panel, Metal-Based Drugs 8 (2001) 19–28, https://doi.org/10.1155/MBD.2001.19.

[17] J. Serment-Guerrero, P. Cano-Sanchez, E. Reyes-Perez, F. Velazquez-Garcia, M. E. Bravo-Gomez, L. Ruiz-Azuara, Genotoxicity of the copper antineoplastic coordination complexes casiopeinas, Toxicol. in Vitro 25 (2011) 1376–1384, https://doi.org/10.1016/J.TIV.2011.05.008.

[18] R. Galindo-Murillo, J.C. García-Ramos, L. Ruiz-Azuara, T.E. Cheatham, F. Cortés-Guzmán, Intercalation processes of copper complexes in DNA, Nucleic Acids Res. 43 (2015) 5364–5376, https://doi.org/10.1093/NAR/GKV467.

[19] Í.P. de Souza, A.C.C. de Melo, B.L. Rodrigues, A. Bortoluzzi, S. Poole, Z. Molphy, V. McKee, A. Kellett, R.B. Fazzi, A.M. da Costa Ferreira, E.C. Pereira-Maia, Antitumor copper(II) complexes with hydroxyanthraquinones and N,N-heterocyclic ligands, J. Inorg. Biochem. 241 (2023) 112121, https://doi.org/10.1016/J.JINORGBIO.2023.112121.

[20] S. Masuri, P. Vaňhara, M.G. Cabiddu, L. Moráň, J. Havel, E. Cadoni, T. Pivetta, Copper(II) phenanthroline-based complexes as potential anticancer drugs: a walkthrough on the mechanisms of action, Molecules 27 (2022) 49, https://doi.org/10.3390/MOLECULES27010049.

[21] V. Scalcon, R. Bonsignore, J. Aupič, S.R. Thomas, A. Folda, A.A. Heidecker, A. Pöthig, A. Magistrato, A. Casini, M.P. Rigobello, Exploring the anticancer activity of tamoxifen-based metal complexes targeting mitochondria, J. Med. Chem. 66 (2023) 9823–9841, https://doi.org/10.1021/acs.jmedchem.3c00617.

[22] H.Q. Zhang, X. Lu, H. Liang, Z.F. Chen, Copper(II) complexes with plumbagin and bipyridines target mitochondria for enhanced chemodynamic cancer therapy, J. Inorg. Biochem. 251 (2024) 112432, https://doi.org/10.1016/J.JINORGBIO.2023.112432.

[23] K. Singh, J. Northcote-Smith, K. Singh, K. Suntharalingam, Cancer stem cell activity of copper(II)-terpyridine complexes with aryl sulfonamide groups, Dalton Trans. 52 (2023) 9694–9704, https://doi.org/10.1039/D3DT01294H.

[24] P.B. Osei, J. Northcote-Smith, J. Fang, K. Singh, F. Ortu, K. Suntharalingam, The bulk breast cancer cell and breast cancer stem cell activity of binuclear copper(II)-phenanthroline complexes, Chem. A Eur. J. 29 (2023) e202301188, https://doi.org/10.1002/CHEM.202301188.

[25] Y. Yang, F.F. Guo, C.F. Chen, Y.L. Li, H. Liang, Z.F. Chen, Antitumor activity of synthetic three copper(II) complexes with terpyridine ligands, J. Inorg. Biochem. 240 (2023) 112093, https://doi.org/10.1016/J.JINORGBIO.2022.112093.

[26] K. Singh, J. Northcote-Smith, X. Feng, K. Singh, K. Suntharalingam, The anti-cancer stem cell properties of copper(II)-terpyridine complexes with attached salicylaldehyde moieties, ChemBioChem (2024), https://doi.org/10.1002/cbic.202400703.

[27] X. Man, W. Li, M. Zhu, S. Li, G. Xu, Z. Zhang, H. Liang, F. Yang, Rational Design of a Hetero-multinuclear gadolinium(III)–copper(II) complex: integrating magnetic resonance imaging, photoacoustic imaging, mild photothermal therapy, chemotherapy and immunotherapy of Cancer, J. Med. Chem. 67 (2024) 15606–15619, https://doi.org/10.1021/acs.jmedchem.4c01273.

[28] K. Ohui, E. Afanasenko, F. Bacher, R.L.X. Ting, A. Zafar, N. Blanco-Cabra, E. Torrents, O. Dömötör, N.V. May, D. Darvasiova, É.A. Enyedy, A. Popović-Bijelić, J. Reynisson, P. Rapta, M.V. Babak, G. Pastorin, V.B. Arion, New water-soluble copper(II) complexes with morpholine–thiosemicarbazone hybrids: insights into the anticancer and antibacterial mode of action, J. Med. Chem. 62 (2019) 512–530, https://doi.org/10.1021/acs.jmedchem.8b01031.

[29] A. Sîrbu, O. Palamarciuc, M.V. Babak, J.M. Lim, K. Ohui, E.A. Enyedy, S. Shova, D. Darvasiová, P. Rapta, W.H. Ang, V.B. Arion, Copper(II) thiosemicarbazone complexes induce marked ROS accumulation and promote nrf2-mediated antioxidant response in highly resistant breast cancer cells, Dalton Trans. 46 (2017) 3833–3847, https://doi.org/10.1039/C7DT00283A.

[30] D. Fabra, J. Melones-Herrero, J. Velazquez-Gutierrez, A.I. Matesanz, P.D. Aliseda, S. Figueiras, F. Aguilar-Rico, C. Calés, I. Sánchez-Pérez, A.G. Quiroga, A select thiosemicarbazone copper(II) complex induces apoptosis in gastric cancer and targets cancer stem cells reducing pluripotency markers, Eur. J. Med. Chem. 280 (2024) 116994, https://doi.org/10.1016/J.EJMECH.2024.116994.

[31] A. Hussain, M.F. AlAjmi, M.T. Rehman, S. Amir, F.M. Husain, A. Alsalme, M. A. Siddiqui, A.A. AlKhedhairy, R.A. Khan, Copper(II) complexes as potential anticancer and nonsteroidal anti-inflammatory agents: in vitro and in vivo studies, Sci. Rep. 9 (1) (2019) 1–17, https://doi.org/10.1038/s41598-019-41063-x.

[32] Q. Peña, G. Sciortino, J.-D. Maréchal, S. Bertaina, A.J. Simaan, J. Lorenzo, M. Capdevila, P. Bayón, O. Iranzo, Ò. Palacios, Copper(II) N, N, O -chelating complexes as potential anticancer agents, Inorg. Chem. 60 (2021) 2939–2952, https://doi.org/10.1021/acs.inorgchem.0c02932.

[33] F. Zhao, W. Wang, W. Lu, L. Xu, S. Yang, X.M. Cai, M. Zhou, M. Lei, M. Ma, H.J. Xu, F. Cao, High anticancer potency on tumor cells of dehydroabietylamine Schiff-base derivatives and a copper(II) complex, Eur. J. Med. Chem. 146 (2018) 451–459, https://doi.org/10.1016/J.EJMECH.2018.01.041.

[34] J.O. Pinho, I.V. da Silva, J.D. Amaral, C.M.P. Rodrigues, A. Casini, G. Soveral, M. M. Gaspar, Therapeutic potential of a copper complex loaded in pH-sensitive long circulating liposomes for colon cancer management, Int. J. Pharm. 599 (2021) 120463, https://doi.org/10.1016/J.IJPHARM.2021.120463.

[35] A. Erxleben, Interactions of copper complexes with nucleic acids, Coord. Chem. Rev. 360 (2018) 92–121, https://doi.org/10.1016/J.CCR.2018.01.008.

[36] C. Molinaro, A. Martoriati, L. Pelinski, K. Cailliau, Copper complexes as anticancer agents targeting topoisomerases I and II, Cancers 12 (2020) 2863, https://doi.org/10.3390/CANCERS12102863.

[37] P. Ji, P. Wang, H. Chen, Y. Xu, J. Ge, Z. Tian, Z. Yan, Potential of copper and copper compounds for anticancer applications, Pharmaceuticals 16 (2023) 234, https://doi.org/10.3390/PH16020234.

[38] Z. Zhang, H. Wang, M. Yan, H. Wang, C. Zhang, Novel copper complexes as potential proteasome inhibitors for cancer treatment, Mol. Med. Rep. 15 (2017) 3–11, https://doi.org/10.3892/MMR.2016.6022.

[39] G. Farine, C. Migliore, A. Terenzi, F. Lo Celso, A. Santoro, G. Bruno, R. Bonsignore, G. Barone, On the G-Quadruplex binding of a new class of nickel(II), copper(II), and zinc(II) Salphen-like complexes, Eur, J. Inorg. Chem. 2021 (2021) 1332–1336, https://doi.org/10.1002/ejic.202100067.

[40] R. Bonsignore, F. Russo, A. Terenzi, A. Spinello, A. Lauria, G. Gennaro, A.M.A. M. Almerico, B.K.B.K. Keppler, G. Barone, The interaction of Schiff Base complexes of nickel(II) and zinc(II) with duplex and G-quadruplex DNA, J. Inorg. Biochem. 178 (2018) 106–114, https://doi.org/10.1016/j.jinorgbio.2017.10.010.

[41] R. Bonsignore, A. Terenzi, A. Spinello, A. Martorana, A. Lauria, A.M. Almerico, B. K. Keppler, G. Barone, G-quadruplex vs. duplex-DNA binding of nickel(II) and zinc (II) Schiff base complexes, J. Inorg. Biochem. 161 (2016), https://doi.org/10.1016/j.jinorgbio.2016.05.010.

[42] A. Terenzi, R. Bonsignore, A. Spinello, C. Gentile, A. Martorana, C. Ducani, B. Högberg, A.M. Almerico, A. Lauria, G. Barone, Selective G-quadruplex stabilizers: Schiff-base metal complexes with anticancer activity, RSC Adv. 4 (2014) 33245–33256, https://doi.org/10.1039/C4RA05355A.

[43] D. Varshney, J. Spiegel, K. Zyner, D. Tannahill, S. Balasubramanian, The regulation and functions of DNA and RNA G-quadruplexes, Nat. Rev. Mol. Cell Biol. 21 (2020) 459–474, https://doi.org/10.1038/s41580-020-0236-x.

[44] J. Spiegel, S. Adhikari, S. Balasubramanian, The structure and function of DNA G-quadruplexes, Trends Chem. 2 (2020) 123–136, https://doi.org/10.1016/j.trechm.2019.07.002.

[45] F. Li, D. Hu, Y. Yuan, B. Luo, Y. Song, S. Xiao, G. Chen, Y. Fang, F. Lu, Zeolite Y encapsulated cu (II) and Zn (II)-imidazole-salen catalysts for benzyl alcohol oxidation, molecular, Catalysis 452 (2018) 75–82, https://doi.org/10.1016/J.MCAT.2018.04.002.

[46] G. Abruscato, R. Chiarelli, V. Lazzara, D. Punginelli, S. Sugár, M. Mauro, M. Librizzi, V. Di Stefano, V. Arizza, A. Vizzini, M. Vazzana, C. Luparello, In vitro cytotoxic effect of aqueous extracts from leaves and rhizomes of the seagrass *Posidonia oceanica* (L.) Delile on HepG2 liver cancer cells: focus on autophagy and apoptosis, Biology 12 (2023) 616, https://doi.org/10.3390/BIOLOGY12040616/S1.

[47] D. Punginelli, V. Catania, G. Abruscato, C. Luparello, M. Vazzana, M. Mauro, V. Cunsolo, R. Saletti, A. Di Francesco, V. Arizza, D. Schillaci, New bioactive

peptides from the mediterranean seagrass *Posidonia oceanica* (L.) delile and their impact on antimicrobial activity and apoptosis of human cancer cells, Int. J. Mol. Sci. 24 (2023) 5650, https://doi.org/10.3390/IJMS24065650.
[48] T.C. Chou, N. Martin, CompuSyn for Drug Combinations: PC Software and User's Guide: A Computer Program for Quantitation of Synergism and Antagonism in Drug Combinations, and the Determination of IC50 and ED50 and LD50 Values, ComboSyn, Paramus, NJ, 2005. https://www.combosyn.com/.
[49] C. Luparello, R. Branni, G. Abruscato, V. Lazzara, S. Sugár, V. Arizza, M. Mauro, V. Di Stefano, M. Vazzana, Biological and proteomic characterization of the anti-cancer potency of aqueous extracts from cell-free coelomic fluid of *Arbacia lixula* sea urchin in an in vitro model of human hepatocellular carcinoma, J. Mar. Sci. Eng. 10 (2022) 1292, https://doi.org/10.3390/JMSE10091292.
[50] C. Luparello, R. Branni, G. Abruscato, V. Lazzara, L. Drahos, V. Arizza, M. Mauro, V. Di Stefano, M. Vazzana, Cytotoxic capability and the associated proteomic profile of cell-free coelomic fluid extracts from the edible sea cucumber Holothuria tubulosa on HepG2 liver cancer cells, EXCLI J. 21 (2022) 722–743, https://doi.org/10.17179/EXCLI2022-4825.
[51] A. Santoro, J.S. Calvo, M.D. Peris-Díaz, A. Krężel, G. Meloni, P. Faller, The glutathione/metallothionein system challenges the design of efficient O2-activating copper complexes, Angew. Chem. Int. Ed. 59 (2020) 7830–7835, https://doi.org/10.1002/ANIE.201916316.
[52] D.D. DeFord, D.N. Hume, The determination of consecutive formation constants of complex ions from polarographic data, J. Am. Chem. Soc. 73 (1951) 5321–5322, https://doi.org/10.1021/JA01155A093/ASSET/JA01155A093.FP.PNG_V03.
[53] J.J. Lingane, Interpretation of the polarographic waves of complex metal ions, Chem. Rev. 29 (1941) 1–35, https://doi.org/10.1021/cr60092a001.
[54] P.A. Mardini Farias, M.B. Rodrigues Bastos, Electrochemical behavior of copper(II) salen in aqueous phosphate buffer at the mercury electrode, Int. J. Electrochem. Sci. 4 (2009) 458–470, https://doi.org/10.1016/S1452-3981(23)15156-X.
[55] D. Niu, D. Wang, L. Fan, Z. Liu, M. Chen, W. Zhang, Y. Liu, J. Xu, Y. Liu, The copper (II) complex of salicylate phenanthroline inhibits proliferation and induces apoptosis of hepatocellular carcinoma cells, Environ. Toxicol. 38 (2023) 1384–1394, https://doi.org/10.1002/TOX.23771.
[56] M.L. Low, C.W. Chan, P.Y. Ng, I.H. Ooi, M.J. Maah, S.M. Chye, K.W. Tan, S.W. Ng, C.H. Ng, Ternary and binary copper(II) complexes: synthesis, characterization, ROS-inductive, proteasome inhibitory, and anticancer properties, J. Coord. Chem. 70 (2017) 223–241, https://doi.org/10.1080/00958972.2016.1260711.
[57] M.A.M.A. Girasolo, L. Tesoriere, G. Casella, A. Attanzio, M.L.M.L. Capobianco, P. Sabatino, G. Barone, S. Rubino, R. Bonsignore, A novel compound of triphenyltin (IV) with N-tert-butoxycarbonyl-L-ornithine causes cancer cell death by inducing a p53-dependent activation of the mitochondrial pathway of apoptosis, Inorg. Chim. Acta 456 (2017) 1–8, https://doi.org/10.1016/j.ica.2016.11.012.
[58] L. Lu, Y. Zhang, X. Tan, Y. Merkher, S. Leonov, L. Zhu, Y. Deng, H. Zhang, D. Zhu, Y. Tan, Y. Fu, T. Liu, Y. Chen, Emerging mechanisms of pyroptosis and its therapeutic strategy in cancer, Cell Death Dis. 8 (1) (2022) 1–13, https://doi.org/10.1038/s41420-022-01101-6.
[59] C. Rogers, D.A. Erkes, A. Nardone, A.E. Aplin, T. Fernandes-Alnemri, E.S. Alnemri, Gasdermin pores permeabilize mitochondria to augment caspase-3 activation during apoptosis and inflammasome activation, Nat. Commun. 10 (1) (2019) 1–17, https://doi.org/10.1038/s41467-019-09397-2.
[60] J.D. Ly, D.R. Grubb, A. Lawen, The mitochondrial membrane potential (δψm) in apoptosis; an update, Apoptosis 8 (2003) 115–128, https://doi.org/10.1023/A:1022945107762.
[61] I.J. Furlong, C. Lopez Mediavilla, R. Ascaso, A. Lopez Rivas, M.K.L. Collins, Induction of apoptosis by valinomycin: mitochondrial permeability transition causes intracellular acidification, Cell Death Differ. 5 (1998) 214–221, https://doi.org/10.1038/SJ.CDD.4400335.
[62] Y.S. Bae, H. Oh, S.G. Rhee, Y. Do Yoo, Regulation of reactive oxygen species generation in cell signaling, Mol. Cell 32 (2011) 491–509, https://doi.org/10.1007/S10059-011-0276-3.
[63] J. Jiang, J.J. Briedé, D.G.J. Jennen, A. Van Summeren, K. Saritas-Brauers, G. Schaart, J.C.S. Kleinjans, T.M.C.M. de Kok, Increased mitochondrial ROS formation by acetaminophen in human hepatic cells is associated with gene expression changes suggesting disruption of the mitochondrial electron transport chain, Toxicol. Lett. 234 (2015) 139–150, https://doi.org/10.1016/J.TOXLET.2015.02.012.